ISSN 0023-1584, Kinetics and Catalysis, 2008, Vol. 49, No. 6, pp. 873–885. © Pleiades Publishing, Ltd., 2008.
Original Russian Text © Z.R. Ismagilov, N.V. Shikina, S.A. Yashnik, A.N. Zagoruiko, S.R. Khairulin, M.A. Kerzhentsev, V.N. Korotkikh, V.N. Parmon, B.I. Brainin, V.M. Zakharov, O.N. Favorskii, 2008, published in Kinetika i Kataliz, 2008, Vol. 49, No. 6, pp. 922–935.

Development and Testing of Granular Catalysts for Combustors of Regenerative Gas Turbine Plants

Z. R. Ismagilov[a], N. V. Shikina[a], S. A. Yashnik[a], A. N. Zagoruiko[a], S. R. Khairulin[a], M. A. Kerzhentsev[a], V. N. Korotkikh[a], V. N. Parmon[a], B. I. Brainin[b], V. M. Zakharov[b], and O. N. Favorskii[b]

[a] *Boreskov Institute of Catalysis, Siberian Branch, Russian Academy of Sciences, Novosibirsk, 630090 Russia*
[b] *Central Institute of Aviation Motors, Moscow, 111116 Russia*
e-mail: zri@catalysis.ru
Received March 28, 2008

Abstract—Two types of granular catalysts for effective methane combustion in combustors of gas turbine plants (GTPs) were developed: (1) catalysts based on noble metals with a low Pd content (1–2 wt %), characterized by a low methane ignition temperature, and (2) catalysts based on manganese oxides and hexaaluminates, which have an increased thermal stability. The methane oxidation kinetics was investigated, and combustion in the catalyst chamber of the GTP was simulated. For optimizing the combustion technology, the following two-step process using a combined catalytic package is suggested. The inlet zone of the combustor is filled with a highly active Pd catalyst, which initiates methane oxidation and ensures that the temperature at the exit of this zone is the initial temperature of methane combustion. This takes place in the next zone, which is filled with an oxide catalyst tolerant to high temperatures. The pilot testing of the catalysts was carried out in a model catalytic combustor. The results are in satisfactory agreement with calculated data. Long-term tests indicate the high stability of the catalysts. The Pd catalyst was demonstrated to retain its high activity and to provide an ignition temperature of 240°C. The initial activity of the hexaaluminate-based catalysts remains unchanged after tests at 930°C. The use of a combined charge of the palladium (7–15%) and manganese (85–93%) catalysts in the model GTP combustor allows a high natural gas combustion efficiency to be achieved at a low level of hazardous emissions (NO_x, 0–1 ppm; CO, 1–3 ppm; hydrocarbons, 3–10 ppm).

DOI: 10.1134/S0023158408060128

The problem of the environmental effect of power plants is gaining increasing importance. Ecological assessment of power-producing gas turbine plants (GTPs) must necessarily take into account the level of atmospheric emissions, such as nitrogen oxides, carbon monoxide, and hydrocarbons. Nitrogen oxides are the most hazardous components of the gas turbine combustion gas from the standpoint of environmental consequences.

A promising approach to the problem of reducing hazardous emissions, primarily nitrogen oxides, is catalytic fuel combustion in various apparatuses, including gas turbines [1–4]. Use of catalytic combustion in gas turbines was suggested in the early 1970s [5, 6], and the investigations that followed confirmed that this is a promising way. In catalytic combustion in industrial gas turbines, the NO_x emission level is lower than 3 ppm and the CO and hydrocarbon emission levels are below 10 ppm [7].

The most available fuel for GTPs is natural gas, which consists largely of methane, which is the least readily oxidizable hydrocarbon. Therefore, it is necessary to produce catalysts capable of initiating methane oxidation at minimum possible temperatures and of withstanding long-term exposure to temperatures above 930°C.

It is well known that catalysts based on noble metals are the most active in oxidation reactions. They can initiate combustion at low temperatures, but it is inappropriate to use them above 750°C because of the high volatility of the noble metals [8]. Use of palladium as the active component in the high-temperature oxidation of methane is the most promising. This is because palladium has a high specific activity in this reaction [9, 10] and a relatively low volatility in comparison with the other noble metals, as was determined by studying the interaction of the metals with oxygen at 730–1730°C [11]. It is these properties of palladium that attract researchers' interest to its behavior in the methane oxidation reaction. It is well known that, up to 800°C, palladium exists as PdO_x, which undergoes reduction to palladium metal as the temperature is further raised. This reaction is reversible, so a decrease in temperature leads to the reoxidation of Pd to PdO_x in air. As a consequence, the temperature dependence of the methane conversion always shows a hysteresis [12]. There is still no consensus as to what form of oxidized palladium—bulk PdO, Pd with oxygen chemisorbed on its surface,

Table 1. Physicochemical properties of the spherical and ring-shaped aluminum oxides

Property	Spherical Al_2O_3	Ring-shaped Al_2O_3
Diameter, mm	2.2–2.5	7.5
Length, mm	–	7.5
Inner diameter, mm	–	2.5
Bulk density, g/cm^3	0.8	0.7
Pore volume (H_2O), cm^3/g	0.45	0.45
Specific surface area, m^2/g	180	200
Crush strength under static conditions, kg/cm^2	270	23
Phase composition	γ-Al_2O_3	60% γ-Al_2O_3 40% χ-Al_2O_3

or Pd particles covered by PdO [13–18]—is the most active in combustion.

Supporting of palladium on a substrate, primarily γ- or α-Al_2O_3 or Al_2O_3 modified with rare-earth element oxides, raises the activity and thermal stability of the catalyst through an increase in the degree of dispersion of the active component and in its aggregation stability [19–25].

Alternative catalytic systems for methane combustion are catalysts based on hexaaluminates and transition metal oxides. Hexaaluminates are the class of compounds with the general formula $AB_xAl_{12-x}O_{19}$, where A is a rare-earth or alkaline-earth metal, such as La and Ba, and B is a transition metal with an atomic radius comparable to the radius of aluminum (B = Mn, Co, Fe, Cr, Ni) [26, 27]. Hexaaluminates form from oxides at temperatures above 1200°C, and this is why they are very stable up to high temperatures. The specific surface area of hexaaluminates and, accordingly, their activity in methane oxidation depend on the synthesis process [28]. However, irrespective of their specific surface area, the hexaaluminates are much less active than the palladium catalysts. In view of this, there have been attempts to enhance the catalytic activity of hexaaluminates by introducing Pd [29]. In our earlier work [30], it was shown that introducing 0.5 wt % Pd into the hexaaluminate $(Mn,Mg)LaAl_{11}O_{19}$ affords a significant activity rise owing to the 110°C decrease in the 50% methane conversion temperature (T_{50}). In addition, a synergistic effect in the Pd–$(Mn,Mg)LaA_{11}O_{19}$ system was detected.

It was demonstrated earlier that stable catalysts based on manganese oxides can be prepared [31]. The activity of these catalysts in hydrocarbon oxidation can be enhanced by their calcination at 900–1100°C. In our works [32, 33], it was found that Mn–Al–O catalysts supported on γ-Al_2O_3 containing χ-Al_2O_3 and modified with Mg, La, or Ce are more active and thermally more stable (up to 1300°C) than the same catalysts supported on pure γ-Al_2O_3. We believe that the high degree of disorder of the χ-Al_2O_3 structure in comparison with γ-Al_2O_3 favors deeper interaction of manganese and modifiers with the support at the impregnation and low-temperature calcination stages. This yields Mn–Al–O compounds of complex composition (solid solutions and/or hexaaluminates) at 1300°C, due to which the catalysts are stable and highly active in methane oxidation.

Abroad, gas turbine catalysts are now produced as foil blocks made from corrosion-resistant alloys. The foil is coated with a porous substrate and an active component based on platinum and/or palladium [34–36]. The disadvantage of these catalysts is their high platinum metal content (above 5–10 wt %) and the operating temperature range being limited to 900°C.

The purpose of this work was to develop granular catalysts for methane oxidation and to optimize the design of the low-noble-metal catalyst package for natural gas (methane) combustion in the catalyst chamber of the gas turbine in order to minimize the NO_x, CO, and unburned hydrocarbon emissions. Optimal catalytic systems were suggested, their physicochemical properties and the methane oxidation kinetics on the catalysts were studied, and methane combustion in the catalytic combustor (CC) was simulated for different compositions of the catalytic package and different testing conditions. Based on the experimental data obtained, the catalytic package design was optimized and pilot tests on a CC model were carried out.

EXPERIMENTAL

Catalyst Preparation

$Pd–Ce–Al_2O_3$. In catalyst preparation, we used γ-alumina supports as spheres and rings. Their characteristics are presented in Table 1. Spherical γ-Al_2O_3 was used in the experiments on catalyst composition optimization. For this purpose, different Pd precursors were tested. The ring-shaped support was used to prepare a pilot batch of the catalyst by the optimal procedure.

The catalysts on the spherical support contained 12 wt % CeO_2 and 1 wt % Pd. They were prepared by the incipient-wetness impregnation of the support with a cerium nitrate ($Ce(NO_3)_3 \cdot 6H_2O$) solution and then with a Pd precursor solution. The precursors were water solutions of H_2PdCl_4, $[Pd(NH_3)_4]Cl_2$, $[Pd(NH_3)_4](NO_3)_2$, and $Pd(NO_3)_2$ and an acetone solution of $Pd(Ac)_2$. Before being loaded with palladium, the alumina support modified with cerium was calcined at 600°C. After supporting of palladium, it was additionally calcined at 1000°C.

The catalyst on the ring-shaped support contained 12 wt % CeO_2 and 2 wt % Pd. It was prepared in the same way as the catalysts on the spherical support. The Pd precursor was an aqueous $Pd(NO_3)_2$ solution. The pilot batch of the catalyst was designated IK-12-60-2.

$MnO_x–Al_2O_3$. The catalyst was prepared on the ring-shaped support by the incipient-wetness impregnation

of the support with an aqueous manganese nitrate ($Mn(NO_3)_2 \cdot 6H_2O$) solution. It contained 11 wt % manganese oxides in terms of MnO_2. The catalyst calcination temperature was 900°C. It was similar in composition to the commercial catalyst IKT-12-40; for this reason, its pilot batch is hereafter designated IKT-12-40A.

MnO_x–La_2O_3–Al_2O_3. This catalyst was prepared on the ring-shaped support by successive incipient-wetness impregnation of alumina with lanthanum and manganese nitrate solutions using the procedure described in [30]. It contained 8–11 wt % manganese in terms of MnO_2 and 10–12 wt % lanthanum in terms of La_2O_3. These concentrations of manganese and lanthanum are sufficient to ensure a high catalytic activity and stability of the catalyst [30]. The calcination temperature was 1000°C, lower than was used in our previous study [30] and was equal to the onset temperature of hexaaluminate phase formation. This allowed us to increase the specific surface area of the sample. The pilot catalyst batch was designated IK-12-61.

Pd–MnO_x–La_2O_3–Al_2O_3. This catalyst was prepared on the ring-shaped support by successive incipient-wetness impregnation with lanthanum and manganese nitrate solutions. Next, the samples were dried and calcined at 400°C. Thereafter, the samples were loaded with a palladium nitrate solution by capillary impregnation. Final calcination was carried out at 1000°C. The resulting catalyst contained 8–11 wt % Mn in terms of MnO_2, 10–12 wt % La in terms of La_2O_3, and was 0.65 wt % Pd. The pilot batch of the catalyst was designated IK-12-62-2.

Testing of the Catalysts

The catalysts were tested using a laboratory setup for methane oxidation, a pilot plant for natural gas combustion (Boreskov Institute of Catalysis, Siberian Branch, Russian Academy of Sciences), and a gas turbine model combustor (Central Institute of Aviation Motors).

The laboratory tests were carried out in a flow quartz reactor using a catalyst size fraction of 0.5–1.0 mm at a GHSV (V_0) of 1000 to 48000 h^{-1}. The gas mixture contained 1 vol % CH_4 in air. The stoichiometric excess of O_2 was calculated as

$$\alpha = \frac{(100 - C_{CH_4}) \times 0.21}{2},$$

where C_{CH_4} is the volumetric concentration of methane in the reaction mixture, 0.21 is the O_2 volume fraction in air, and 2 is the stoichiometric coefficient of O_2 in the chemical equation

$$CH_4 + 2O_2 = CO_2 + 2H_2O.$$

For the above composition of the reaction mixture, $\alpha = 10.4$.

The reaction products were analyzed by gas chromatography. From the reactant and product concentrations, the CH_4 conversion (in percent) was calculated as

$$x_{CH_4} = \frac{C^0_{CH_4} - C_{CH_4}}{C^0_{CH_4}} \times 100,$$

where $C^0_{CH_4}$ and C_{CH_4} are the methane concentrations (vol %) in the initial reaction mixture and in the reaction products, respectively. Based on experimental data, we plotted the temperature dependence of the methane conversion.

The pilot plant tests were carried out in a tubular flow reactor, into which 100 cm^3 of a catalyst was charged. The bed height was 40 mm. The methane concentration of the inlet was 5.2–7.0 vol %, and the GHSV was $V_0 = 4300\ h^{-1}$. The catalytic activity was estimated as the "ignition" temperature (T_{ign}) and as the completeness of natural gas combustion with air. For this purpose, the products were analyzed using an EKOM gas analyzer. The determination accuracy was 1 ppm for both carbon monoxide and NO_x.

In the model CC, the inlet temperature was 570°C (840 K), the gas velocity before the catalytic package (midlength flow velocity in the chamber) was ~2 m/s, and the air excess α factor was 6.6 to 10.0.

The oxidation products were analyzed at the outlet of the CC with a gas analyzer complex (Beckman, United States) by measuring the volume concentrations of CO (IR absorption), hydrocarbons (flame ionization detector), and NO_x (chemiluminescence technique).

Characterization of the Catalysts

The distribution of Pd in the catalyst grain cross section was studied by X-ray microanalysis using an MAR-3 instrument. The catalyst grain was secured in epoxy resin and was ground to half-height. Graphite was sprayed onto the specimen surface for charge removal. The specimen was moved with a velocity of 10–40 μm/min.

The textural characteristics of the catalysts (specific surface area, S_{sp}, m^2/g; pore volume, V_{pore}, cm^3/g) were determined by adsorption techniques using an ASAP-2400 device.

The phase composition of the catalyst was studied by X-ray diffraction using an HZG–4 diffractometer (monochromated CoK_α radiation). For phase identification the X-ray database of ICPDS was used.

The mechanical strength of the catalysts (P, kg/cm^2) was measured using an MP–9S instrument, which is intended for measuring the strength of porous bodies under static conditions.

Reaction Kinetics

We assumed that, in excess oxygen, only total methane oxidation to CO_2 and H_2O takes place. The overall reaction rate was described by the equation

$$w = k_0(1-\varepsilon)\exp\left(-\frac{E}{RT}\right)C_{CH_4}\left(\frac{P}{P_0}\right), \quad (1)$$

where k_0 is a preexponential factor of the rate constant (s^{-1}), E is the activation energy (J/mol), R is the universal gas constant (J mol^{-1} K^{-1}), T is the reaction temperature (K), ε is the void fraction of the catalyst bed, C_{CH_4} is the methane concentration (in mole fractions), P is the current working pressure (atm), and P_0 is the initial pressure (in this case, 1 atm).

Mathematical Modeling

The catalyst bed was modeled using the steady-state model of the adiabatic plug-flow reactor in terms of heat and mass:

$$u\frac{\partial C_{CH_4}}{\partial l} = -w = \beta(C^*_{CH_4} - C_{CH_4}), \quad (2)$$

$$u\frac{\partial T_g}{\partial l} = xC^{in}_{CH_4}\Delta T_{ad} = \frac{\alpha}{c_p}(T_{cat} - T_g), \quad (3)$$

$$C_i = C_i^{in}, \quad T = T_{in}, \quad (4)$$

where u is the linear velocity of the gas in the reactor (m/s) reduced to the normal conditions and to the total cross-sectional area of the reactor; l is the coordinate along the bed height (m); x is the methane conversion; $C^*_{CH_4}$ and C_{CH_4} are the methane concentrations on the catalyst grain surface and in the gas flow, respectively; β is the mass transfer coefficient for methane (s^{-1}); T_g and T_{cat} are the gas and catalyst temperatures, respectively (K); ΔT_{ad} is the adiabatic heating (K); α is the heat transfer coefficient (W m^{-3} K^{-1}); c_p is the heat capacity of the gas (J m^{-3} K^{-1}); and the subscript or superscript *in* stands for the reactor inlet.

The reaction rate in the kinetically controlled region was determined using Eq. (1) and the above kinetic parameters. In the calculation of the apparent reaction rate, we took into account the internal and external diffusion limitations. In view of the presence of excess oxygen, we took into account only the limitations for methane diffusion.

The internal diffusion limitation was estimated by the Thiele method. For a first-order reaction, the degree of use of the internal surface of the catalyst grain (η) is given by the following equation [37]:

$$\eta = \frac{3}{\varphi}\left(\coth\varphi - \frac{1}{\varphi}\right). \quad (5)$$

Here, the Thiele modulus is

$$\varphi = \frac{r}{3}\sqrt{\frac{k}{D_{eff}}}, \quad (6)$$

where r is the equivalent radius of the catalyst grain (m), k is the reaction rate constant in the kinetically controlled region (s^{-1}), and D_{eff} is the effective diffusion coefficient of methane in the catalyst pores (m^2/s).

The effective diffusion coefficient was calculated by the formula [37]

$$D_{eff} = \Pi\left(\frac{1}{1/D + 1/D_{Kn}}\right), \quad (7)$$

where Π is the permeability coefficient (taken to be 0.2 [37]) and D and D_{Kn} are the molecular and Knudsen diffusion coefficients of methane (m^2/s). D and D_{Kn} were determined using the following equations [37, 38]:

$$D = \frac{4.3\times10^{-7}T_{cat}^{3/2}}{P(\nu_{CH_4}^{1/3} + \nu_{N_2}^{1/3})^2}\sqrt{\frac{1}{M_{CH_4}} + \frac{1}{M_{N_2}}}, \quad (8)$$

$$D_{Kn} = 97r_p\sqrt{\frac{T_{cat}}{M_{CH_4}}}, \quad (9)$$

where ν_{CH_4} and ν_{N_2} are the specific molar volumes of methane and of the dominant gas in the mixture, specifically, nitrogen (cm^3/atom); M_{CH_4} and M_{N_2} are the methane and nitrogen molecular weights; and r_p is the mean pore radius in the catalyst (m). For this catalyst, the mean pore radius was taken to be 170 Å based on porosimetry data.

The apparent reaction rate taking into account the external diffusion limitations was described in terms of the constant k'. For the pseudo-first-order reaction with respect to methane, this constant was calculated as

$$k' = \frac{1}{1/\eta k + 1/\beta}, \quad (10)$$

where β is the mass transfer coefficient for methane (s^{-1}), which can be determined using the following familiar equations [39]:

$$\beta = \frac{\mathrm{Sh}DS_{sp}P}{d_{equiv}}, \quad (11)$$

$$\mathrm{Sh} = A\mathrm{Re}^B\mathrm{Sc}^{0.33}, \quad (12)$$

$$\mathrm{Re} = \frac{u_r d_{equiv}\rho}{\mu}, \quad (13)$$

$$\mathrm{Sc} = \frac{\mu\rho}{D}, \quad (14)$$

where Sh, Re, and Sc are the dimensionless Sherwood, Reynolds, and Schmidt numbers, respectively; D is the molecular-diffusion coefficient of methane in air

Table 2. Physicochemical properties of Pd–Ce–Al_2O_3 catalysts obtained using various palladium precursors

Catalyst no.	Precursor	S_{sp}, m^2/g	V_{por} (H_2O), cm^3/g	Strength, kg/cm^2	Phase composition
1	H_2PdCl_4	80	0.35	275	δ-Al_2O_3, PdO ($D \approx 400$ Å), CeO_2 ($D \approx 210$ Å)
2	$Pd(NH_3)_4Cl_2$	76	0.35	268	δ-Al_2O_3, PdO ($D \approx 200$ Å), CeO_2 ($D \approx 220$ Å)
3	$Pd(NH_3)_4(NO_3)_2$	83	0.35	280	δ-Al_2O_3, PdO ($D \approx 200$ Å), CeO_2 ($D \approx 210$ Å)
4	$Pd(Ac)_2$	75	0.35	283	δ-Al_2O_3, PdO ($D \approx 150$ Å), CeO_2 ($D \approx 210$ Å)
5	$Pd(NO_3)_2$	76	0.35	270	δ-Al_2O_3, PdO ($D \approx 250$ Å), CeO_2 ($D \approx 210$ Å)

Note: The Pd content of the catalysts is 1 wt %, the CeO_2 content is 12 wt %, and the calcination temperature is 1000°C. The particle size D was derived from the coherent-scattering domain size.

(m^2/s); S_{sp} is the specific surface area of the catalyst grains per unit volume of the bed (m^{-1}); d_{equiv} is the equivalent (hydraulic) diameter of the path in the bed (m); A and B are empirical parameters; u_r is the real linear velocity of the gas in the bed (m/s); ρ is the gas density (kg/m^3); and μ is the gas viscosity (N s m^{-2}).

The real velocity of the gas, u_r, was calculated taking into account temperature, pressure, and free bed cross section corrections:

$$u_r = u\frac{T_g}{273}\frac{1}{\varepsilon}\frac{1}{P}. \quad (15)$$

In a similar way, we determined the heat transfer coefficient:

$$\alpha = \frac{\mathrm{Nu}\lambda S_{sp}}{d_{equiv}}, \quad (16)$$

$$\mathrm{Nu} = A\mathrm{Re}^B\mathrm{Pr}^{0.33}, \quad (17)$$

where Nu and Pr are the Nusselt and Prandtl numbers, respectively, and λ is the thermal conductivity of the reacting gas. The empirical parameters A and B in Eqs. (12) and (17) were assigned particular numerical values depending on the type of hydrodynamic regime according to recommendations given in [39].

The gas flow resistance of the catalyst bed was calculated by the formula [40]

$$\Delta P = \xi\frac{L}{d_{equiv}}\frac{\rho u_r^2}{2}, \quad (18)$$

where L is the total bed height (m). The resistance coefficient ξ was calculated using the general formula

$$\xi = \frac{F}{\mathrm{Re}^p}, \quad (19)$$

where the parameters F and p were assigned particular values depending on the Reynolds number according to recommendations given in [40].

The gas velocity in the reactor (u) was determined from the bed geometry and GHSV, applying corrections for the real temperature and pressure. In the estimation of the gas viscosity μ and thermal conductivity λ as a function of temperature, we used reference data [38, 40]. The gas density ρ was calculated using the ideal-gas equation of state applied to air.

The adiabatic heating for methane oxidation was determined by thermodynamic calculations.

RESULTS AND DISCUSSION

Physicochemical Properties of Catalysts and Optimization of Catalyst Compositions

Table 2 lists data characterizing the physicochemical properties of Pd–Ce–Al_2O_3 catalysts 1–5, which differ in the chemical nature of the Pd precursor. The catalysts have similar specific surface areas and pore volumes. The chemical nature of the precursor influences the Pd distribution in the cross section of the catalyst grain, which, in turn, has an effect on the Pd particle size. Figure 1 shows the Pd distribution profile in the grains of catalysts 1–5 on the spherical support as determined by the X-ray microprobe method. The signal intensity increases in particular areas as the microprobe moves across the grain, indicating the concentration of Pd there. In catalyst 1, prepared using H_2PdCl_4, the

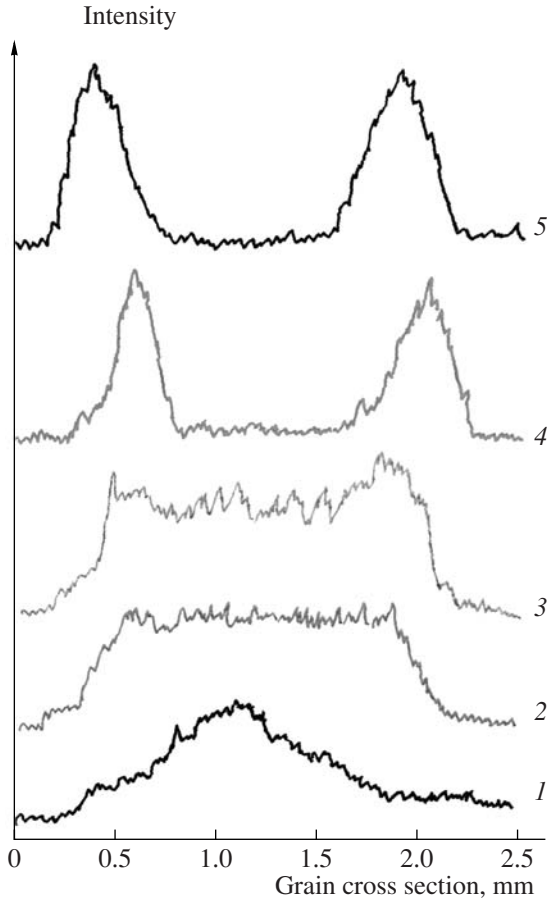

Fig. 1. Palladium distribution profiles for the Pd–Ce–Al_2O_3 catalyst grains prepared using different precursors (X-ray microprobe analysis data): (*1*) H_2PdCl_4, (*2*) $[Pd(NH_3)_4]Cl_2$, (*3*) $[Pd(NH_3)_4](NO_3)_2$, (*4*) $Pd(Ac)_2$, and (*5*) $Pd(NO_3)_2$.

active component is mainly concentrated in the grain center ("egg-yolk" distribution), and this why this catalyst is prone to aggregation and has a low degree of dispersion. Catalysts 2 and 3, prepared from palladium ammine complexes, are characterized by a uniform Pd distribution over the grain and have a higher degree of dispersion (D = 200 Å) than catalyst 1. The use of $Pd(NO_3)_2$ and $Pd(Ac)_2$ solutions as precursors leads to Pd concentrating on the grain surface, that is, to the so-called "egg-shell" distribution (samples 4 and 5). This distribution of the active component is the most preferable for catalysts used in the gas turbines and work at high gas temperatures and linear velocities.

As is demonstrated in Fig. 2, the catalysts with a egg-shell Pd distribution (samples 4 and 5) are the most active in methane oxidation (1 vol % CH_4 + air, V_0 = 24000 h^{-1}). The catalysts with a uniform Pd distribution are less active (samples 2 and 3), and the catalyst with a egg-yolk Pd distribution shows the lowest activity (sample 1).

Based on the data characterizing the degree of dispersion of Pd and the activity of various samples pre-

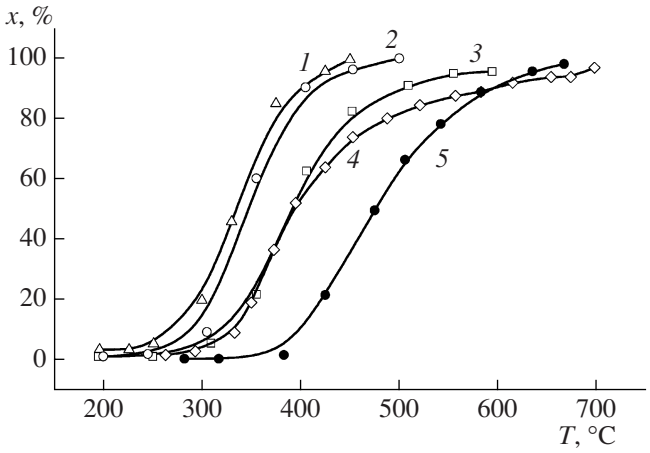

Fig. 2. Temperature dependence of methane conversion (1 vol % CH_4 + air, V_0 = 24000 h^{-1}) on Pd–Ce–Al_2O_3 catalysts prepared using different precursors: (*1*) $Pd(NO_3)_2$, (*2*) $Pd(Ac)_2$, (*3*) $[Pd(NH_3)_4]Cl_2$, (*4*) $[Pd(NH_3)_4](NO_3)_5$, and (*5*) H_2PdCl_4.

pared using the optimal palladium precursor ($Pd(NO_3)_2$), we produced a pilot batch of the Pd–Ce–Al_2O_3 catalyst (IK-12-60-2) on the ring-shaped support. Its physicochemical properties are listed in Table 3. Figure 3 shows the distribution of elements in the cross section of the ring wall as determined by the X-ray microprobe method. Aluminum and cerium are seen to be uniformly distributed over the cross section of the ring wall. The Al and Ce distribution profiles are identical, so partial interaction between aluminum and cerium oxides cannot be ruled out. Palladium concentrates closer to the ring wall surface, much as in the case of the spherical grains.

The catalyst IK-12-60-2 shows high activity in methane oxidation at various GHSV values (1000, 24000, and 48000 h^{-1}), as is demonstrated in Fig. 4.

When developing and optimizing the catalysts based on manganese oxides, including those additionally containing lanthanum and palladium, we investigated how their physicochemical and catalytic properties depend on their chemical composition, the active component and modifier (manganese, lanthanum, palladium, and hexaaluminate phase) contents, the chemical nature of Mn and Pd precursors, the calcination temperature, and the component introduction method [30, 32, 33]. Measuring the catalytic activity of catalyst samples in methane oxidation allowed us to find the optimal catalytic systems, whose properties are listed in Table 3.

The catalysts on the ring-shaped alumina support (IK-12-60-2, IKT-12-40A, IK-12-61, IK-12-62-2) were tested in natural gas combustion at 930°C in the pilot plant at the Boreskov Institute of Catalysis. The results of these tests are presented in Table 4. The catalyst IK-12-60-2 retained its high activity over 100 h: the igni-

Table 3. Physicochemical properties of the initial catalysts on spherical and ring-shaped supports

Catalyst	Calcination temperature, °C	Chemical composition, wt %	Phase composition*	S_{sp}, m^2/g	V_Σ (N_{ads}), cm^3/g	Strength, kg/cm^2
IK-12-60-2	1000	Pd, 2.1 Ce, 10.1	δ-Al_2O_3, CeO_2 (~200 Å, S_{33} = 1100), PdO (~180 and 250 Å, S_{39} = 480)	74	0.26	24
IKT-12-40A	900	Mn, 6.9	Mixture of (δ + γ)-Al_2O_3, α-Al_2O_3, Mn_2O_3	80	0.23	23
IK-12-61	1000	Mn, 6.9 La, 10.1	$MnLaAl_{11}O_{19}$ (S_{37} = 60), $LaAlO_3$, γ-$Al_2O_3^{\#}$	43	0.18	34
IK-12-62-2	1000	Pd, 0.65 Mn, 7.1 La, 9.4	$MnLaAl_{11}O_{19}$ (S_{37}-traces), γ-$Al_2O_3^{\#}$ (a = 7.937 Å), PdO (~400 Å, S_{39} = 70)	48	–	25

* The particle size was derived from the coherent-scattering domain size. Relative phase contents were estimated from peak areas (S_i, arb. units) in diffraction patterns. γ-$Al_2O_3^{\#}$ is a solid solution based on γ-Al_2O_3.

tion temperature was T_{ign} = 240°C, and the reaction products were almost free of CO and NO_x. The manganese-containing catalysts were less active: with these catalysts, T_{ign} and the residual CO and NO_x contents were higher than with IK-12-60-2. However, the initial activity of the catalyst IK-12-61 did not decrease, but even gradually increased during testing: in 200 h, T_{ign} falls from 365 to 350°C, the NO_x concentration in the reaction products remained at the 0–1 ppm level, and the CO concentration decreased from 55 to 34 ppm. The catalyst IK-12-61 modified with 0.65 wt % palladium (IK-12-62-2) allowed us to reduce the ignition temperature of the methane–air mixture almost by 100°C and the CO concentration in the reaction products by more than one order of magnitude. Durability tests suggested that all catalysts are tolerant to high temperatures (up to 930°C) and to the action of the reaction medium. The ignition temperature and the methane–air combustion efficiency remained unchanged at least over 100 h of testing.

The investigation of the physicochemical properties of the initial samples (Table 3) showed that, in IK-12-60-2, the active component PdO is finely dispersed and this allows one to initiate combustion of the methane–air mixture at low temperatures. The initial catalysts based on Mn and La oxides (IK-12-61 and IK-12-62-2) contain the hexaaluminate phase, which is known to be resistant to high temperatures. The durability tests altered the structural and textural characteristics of the catalysts (Table 5). Over the first 50 h of testing, the specific surface area and pore volume of the IK-12-60-2 catalyst decreased because of the coarsening of alumina particles and the onset of α-Al_2O_3 formation via the δ-Al_2O_3–α-Al_2O_3 phase transition under prolonged heating. The active component PdO underwent partial decomposition to Pd^0. In the next 50 h, the textural parameters stabilized and the degree of dispersion of the remaining PdO phase increased. The degree of dispersion of metallic Pd^0 decreased with testing time. The manganese catalysts are more tolerant to high temperatures and are less prone to aggregation than the Pd–Ce catalyst. Some changes in the phase composition of the catalysts occur because of the formation of high-temperature phases, namely, α-Al_2O_3 and a (Mn, Al)Al_2O_4 solid solution in IKT-12-40A and manganese hexaaluminate in IK-12-61 and IK-12-62-2.

The catalytic activity of the hexaaluminate-based samples in the methane oxidation model reaction after 100-h-long testing was similar to the activity of the fresh catalysts: T_{50} is 470–480°C for the catalyst IK-12-61 and 363–380°C for IK-12-62-2 at V_0 = 1000 h^{-1} (Fig. 5). The activity of the catalysts Pd–Ce–Al_2O_3 and MnO_x–Al_2O_3 decreased slightly, and T_{50} increased by 50°C.

Mathematical Modeling

In order to calculate the efficiency of various catalyst package arrangements and optimize the amounts of the catalysts, we investigated the kinetics of methane

Table 4. Results of catalyst durability tests using the natural gas combustion pilot plant at the Boreskov Institute of Catalysis

Catalyst	Test duration, h	T_{ign}, °C	Residual content, ppm	
			CO	NO_x
IK-12-60-2	100	240	0–1	0–1
IKT-12-40A	100	350	84–55	0–1
IK-12-61	200	365–350	55–34	0–1
IK-12-62-2	200	290	2–3	0–1

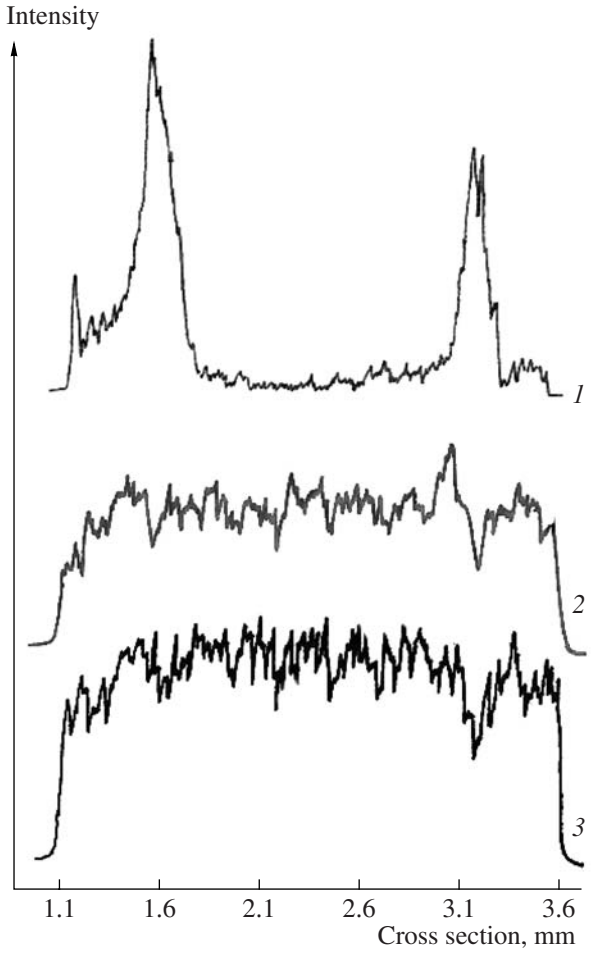

Fig. 3. (*1*) Pd, (*2*) Ce, and (*3*) Al distribution profiles for the catalyst IK-12-60-2 determined by the X-ray microprobe method (the zero point in the *x* axis is the axis of the ring-shaped grain).

oxidation on IK-12-60-2, IKT-12-40A, IK-12-61, and IK-12-62-2 and simulated natural gas combustion in the CC.

In kinetic calculations, we used activity data for the 0.5–1.0 mm size fractions of the catalysts in methane oxidation at V_0 = 1000, 24000, and 48000 h^{-1}. The results obtained by data processing in the plug flow approximation are presented in Table 6.

Initially, we calculated the operating parameters of the reactor charged with one of the most effective Pd-containing catalysts—IK-12-60-2 or IK-12-62-2. In these calculations, we took into account the effects of internal and external diffusion for a reactor with a diameter of 80 mm and a catalyst bed height of 200 to 400 mm. We considered the methane concentration range of 1.5–5.0 vol %, the V_0 range of 9000–40000 h^{-1}, and inlet temperature range of 450–500°C.

With the catalyst IK-12-60-2 alone, complete methane conversion is achieved throughout the above parameter ranges. For the catalyst IK-12-62-2 alone,

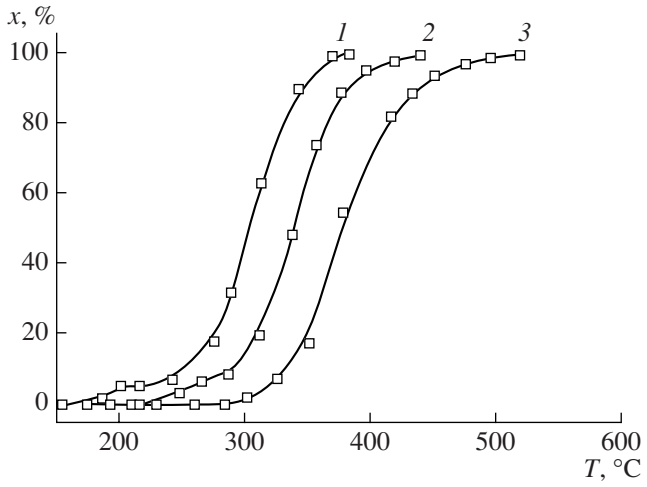

Fig. 4. Temperature dependence of methane conversion (1 vol % CH_4 + air) on the catalyst IK-12-60-2 at V_0 = (*1*) 1000, (*2*) 24000, and (*3*) 48000 h^{-1}.

100% methane conversion throughout the V_0 range is observed at an initial methane concentration of 1.5 vol % and an inlet temperature of 500°C (Fig. 6). At higher methane concentrations, complete methane conversion is achieved at inlet temperatures of 450 and 475°C (not presented in the Figure).

The simulation of combustion on a combined catalytic package was carried out for the IK-12-60-2/IK-12-61 combinations with bed height ratios of 20/180, 30/170, and 40/160 mm. It was supposed that the temperature at the inlet was 450°C and that the initial mixture contained 1.5 vol % methane. For the 20/180 mm combination, we additionally carried out calculations for the mixture containing 3.6 vol % methane. The calculated data are shown in Fig. 7. For the initial methane concentration of 1.5 vol %, complete methane conversion is attained at V_0 < 12000 h^{-1}. For higher V_0, for ensuring complete combustion, it is necessary to increase the bed height of the more active Pd–Ce catalyst IK-12-60-2. For the initial methane concentration of 3.6 vol %, greater adiabatic heating takes place in the first bed and, due to this, complete methane conversion in the 20/180 mm combined bed is observed at V_0 = 5000–35000 h^{-1}.

In a similar way, we carried out the modeling of a combined bed consisting of the IK-12-60-2 and IK-12-62-2 catalysts, varying the height ratio of the constituent beds at a constant total height of 200 mm. The calculation of the gas and catalyst temperature and methane conversion profiles along the catalyst bed height at V_0 = 10000 h^{-1} demonstrated that, under these conditions, methane is almost completely converted in the upstream bed of the IK-12-60-2 catalyst and the gas temperature is linearly related with the methane conversion. The catalyst temperature far exceeds the gas temperature in the zone of high methane conversion rates, and the catalyst temperature maximum occurs in

Table 5. Physicochemical properties of the catalysts after durability tests in natural gas combustion

Catalyst	Test duration, h	Chemical composition, wt %	Phase composition*	S_{sp}, m^2/g	V_Σ (N_{ads}), cm^3/g	Strength, kg/cm^2
IK-12-60-2	50	Pd, 2.1 Ce, 10.1	δ-Al_2O_3, α-Al_2O_3 (traces), CeO_2 (~200 Å, S_{33} = 1100), PdO (~300 Å, S_{39} = 180), Pd° (~300 Å, S_{47} = 120)	42	0.18	21
	100	Pd, 2.0 Ce, 10.4	δ-Al_2O_3, α-Al_2O_3 (traces), CeO_2 (~200 Å, S_{33} = 1100), PdO (~160 Å, S_{39} = 180), Pd° (~500 Å, S_{47} = 80)	38	0.17	19
IKT-12-40A	100	Mn, 6.9	α-Al_2O_3, γ-Al_2O_3-based solid solution $(Mn,Al)Al_2O_4$ (a = 8.151 Å)	66	0.22	19
IK-12-61	30	Mn, 6.7 La, 10.3	$MnLaAl_{11}O_{19}$ (S_{37} = 240), $LaAlO_3$, α-Al_2O_3	41	0.18	30
	50	″	$MnLaAl_{11}O_{19}$ (S_{37} = 250), $LaAlO_3$, α-Al_2O_3	33	0.15	28
	100	″	$MnLaAl_{11}O_{19}$ (S_{37} = 240), $LaAlO_3$, α-Al_2O_3	31	0.13	28
IK-12-62-2	50	Pd, 0.62 Mn, 7.2 La, 9.2	$MnLaAl_{11}O_{19}$ (S_{37} = 230), γ-$Al_2O_3^{\#}$ (a = 7.937 Å), Pd° (S_{41} = 90), PdO (400 Å, S_{39} = 160)	31	–	29
	100	″	$MnLaAl_{11}O_{19}$ (S_{37} = 230), γ-$Al_2O_3^{\#}$ (a = 7.937 Å), Pd^0 (>400 Å, S_{47} = 40), PdO (>400 Å, S_{39} = 160)	30	–	32
	200	″	$MnLaAl_{11}O_{19}$ (S_{37} = 340), γ-$Al_2O_3^{\#}$ (a = 7.937 Å), α-Al_2O_3 (S_{29} = 30), PdO (>400 Å, S_{39} = 180), Pd° (>400 Å, S_{47} = 40)	30	–	35

* The particle size was derived from the coherent-scattering domain size. Relative phase contents were estimated from peak areas (S_i, arb. units) in diffraction patterns. γ-$Al_2O_3^{\#}$ is a solid solution based on γ-Al_2O_3.

the upstream bed. Downstream along the bed height, as the reaction rate and heat evolution decrease, the difference between the gas and catalyst temperatures diminishes and almost vanishes at the bed outlet.

The calculation of the methane conversion profile at V_0 = 10000–60000 h^{-1} and different IK-12-60-2 catalyst bed heights (20 and 40 mm) showed that, with an increase in the volume of this most active catalyst, the methane conversion increases (Fig. 8). Formal interpretation of the simulation results might lead to the inference that the bed consisting of the IK-12-60-2 catalyst alone is preferable. However, from the practical standpoint, the combined bed is more advantageous: it allows one to reduce the total palladium content of the catalytic package and, at the same time, to extend its durability by using the thermally more stable catalyst IK-12-62-2 in the high-temperature zone. From these considerations, the optimum package design includes an upstream IK-12-60-2 bed with a height of 20–40 mm.

The simulation of combustion on catalyst grains with various shapes and sizes (spheres, cylinders, rings

Table 6. Kinetic parameters of the total methane oxidation reaction

Catalyst	k_0, s^{-1}	E, kJ/mol
IK-12-60-2	4.36×10^7	81.4
IKT-12-40A	1.09×10^5	71.2
IK-12-61	1.09×10^5	71.2
IK-12-62-2	3.29×10^5	63.8

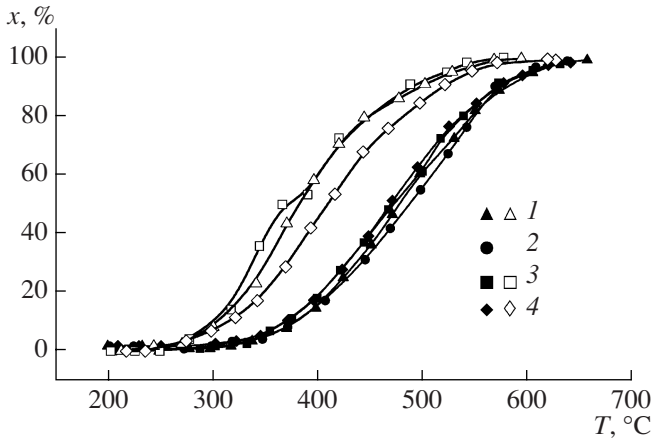

Fig. 5. Temperature dependences of methane conversion (1 vol % CH_4 + air, $V_0 = 1000\ h^{-1}$) on the catalysts IK-12-61 (black points) and IK-12-62-2 (light points): (*1*) fresh sample and (*2–4*) the same sample tested for (*2*) 30, (*3*) 50, and (*4*) 100 h.

with different wall thicknesses) demonstrated that the spherical and cylindrical grains are inappropriate because they produce high pressure losses. The optimal grain shape is a ring. Rings with an outer diameter of 7 mm, a length of 7 mm, a hole diameter of 3 mm ($7 \times 7 \times 3$ mm), and a wall thickness of 2 mm are the most efficient. A further decrease in the catalyst wall thickness has ambiguous consequences: on the one hand, this reduces the internal-diffusion limitations and the flow resistance of the bed; on the other hand, the weight of the catalyst in the bed decreases, eventually diminishing the methane conversion. Furthermore, a decrease in the wall thickness reduces the mechanical strength of the catalyst grains.

Thus, the mathematical calculations demonstrated that the maximum completeness of fuel combustion in the CC is achieved by using the catalyst package IK-12-60-2/IK-12-62-2 (IK-12-61, IKT-12-40A) with the catalysts shaped as rings with dimensions of $7 \times 7 \times 3$ mm and the bed height ratio 20–40/180–160 mm. The process should be carried out at a methane concentration of 1.5 vol % in air and an inlet gas temperature of 450–550°C.

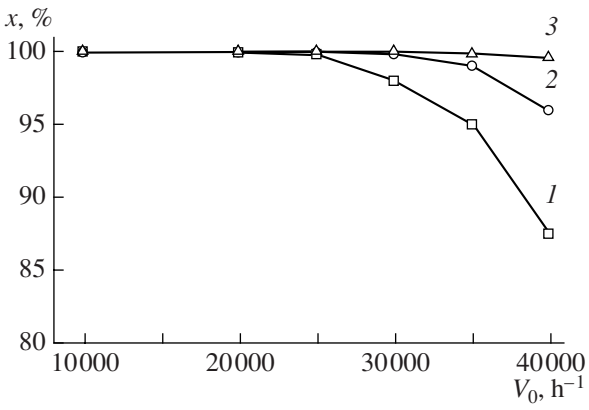

Fig. 6. Methane conversion (1.5 vol %) on the catalyst IK-12-62-2 versus GHSV at inlet temperatures of (*1*) 450, (*2*) 475, and (*3*) 500°C.

Tests in the Model Catalytic Combustor

Pilot batches of the catalysts were tested using an experimental setup including a model CC at the Central Institute of Aviation Motors (Fig. 9). The main design parameters of the CC are described elsewhere [41].

We have already discussed the testing data for homogeneous packages of different catalysts, including IK-12-60-2, IKT-12-40A, and IK-12-61 [41], and have demonstrated that, with these catalysts, the NO_x concentration in the combustion products does not exceed 1 ppm. The regulatory CO and hydrocarbon levels in the waste gas of the GTPs used in the decentralized power supply are on the order of 10 ppm. With individual catalysts, this value is achievable only in a rather narrow range of combustion parameters.

For improvement of natural gas combustion in the gas turbine combustor, it was suggested to use two-stage combustion in combined catalyst beds (catalytic packages). A highly active catalyst containing noble metals is placed in the reactor inlet (ignition) zone. It initiates natural gas oxidation and ensures an exit temperature appropriate for the onset of combustion in the next zone. This second zone is filled with an oxide catalyst tolerant to high temperatures.

The use of the combined catalytic package consisting of 15% IK-12-60-2 and 85% IKT-12-40A (on the bed height basis) allowed us to sharply raise the process

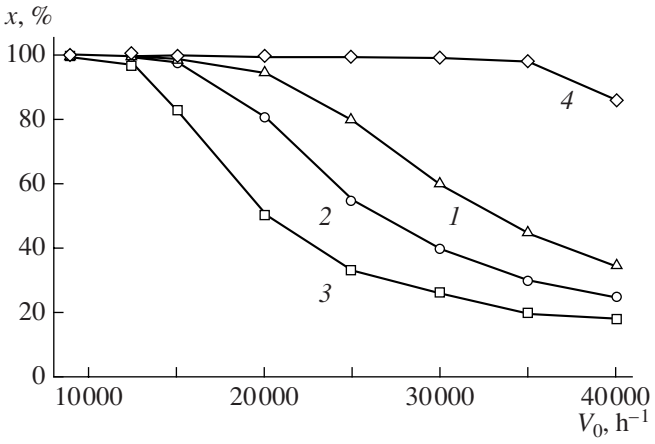

Fig. 7. Methane conversion on the combined catalyst bed IKT-12-60-2/IK-12-61 versus GHSV at an inlet temperature of 450°C and initial methane concentrations of (*1–3*) 1.5 and (*4*) 3.6 vol %. The bed height ratio, mm: (*1*) 40/160, (*2*) 30/170, (*3*) 20/180, and (*4*) 20/180.

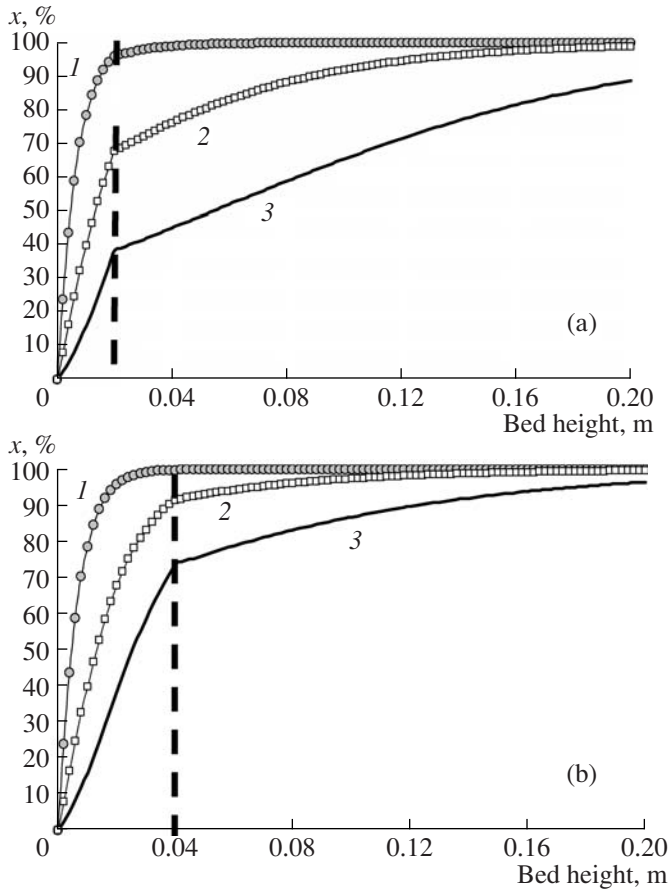

Fig. 8. Methane conversion profiles along the catalyst bed height for IKT-12-60-2/IKT-12-62-2 bed height ratios of (a) 20/180 and (b) 40/160 mm V_0 = (*1*) 10000, (*2*) 40000, and (*3*) 60000 h^{-1}. The catalyst grains are rings with dimensions of 7 × 7 × 3 mm, the inlet temperature is 447°C, the initial methane concentration is 1.5 vol %, and pressure is 1 atm.

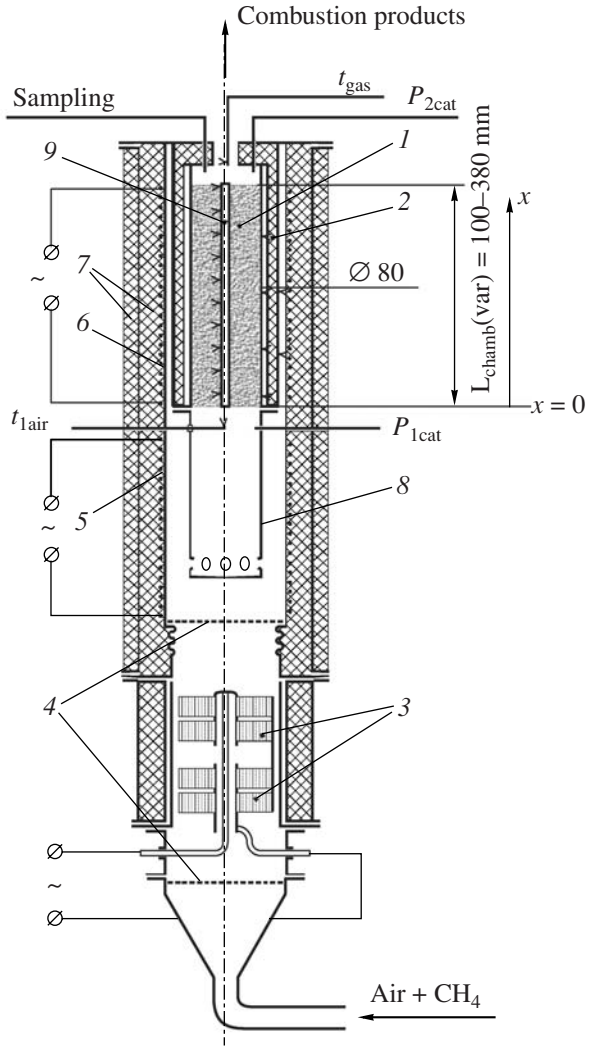

Fig. 9. Model setup with a catalytic combustor: (*1*) catalytic chamber, (*2*) heat shield, (*3*) electric heater of air, (*4*) leveling grid, (*5*) electric heater, (*6*) electric "guard" heater, (*7*) heat insulation, (*8*) mixer, and (*9*) thermal probe.

efficiency in a wide range of chamber operation regimes under given environmental constraints.

An analysis of the first results of combined catalytic package testing in the CC showed that, in some regimes, the Pd catalyst IK-12-60-2 is overheated above 827°C, which can cause the loss of its activity. For this reason, the IK-12-60-2 bed was reduced from 45 to 20 mm and an inert material bed was placed between the two catalysts to screen radiation heat transfer between the catalyst beds. The final catalytic package includes an IK-12-60-2 bed 20 mm in height, an inert bed 20 mm in height, and an IKT-12-40A bed 260 mm in height. At an inlet temperature of 567°C and various methane concentrations, even at the smallest O_2 excess factor of $\alpha = 6.7$, the highest temperature in the IKT-12-60-2 bed does not exceed 727°C (Fig. 10).

With this design of the catalytic package, the completeness of fuel combustion in a wide range of methane–air mixture compositions ($\alpha = 6.7$–10.0) compares well with the world level (Fig. 11).

With the reactor charged with the IK-12-62-2 catalyst alone (0.5 wt % Pd), the hydrocarbons, CO, and NO_x emissions are approximately the same as with the combined catalytic package; however, the combined package is preferable because its total Pd content (0.13 wt %) is significantly lower.

Thus, for increasing the fuel combustion efficiency in the CC of the GTP, it is appropriate to use two types of granular catalysts:

(1) The highly active Pd-based catalyst 2% Pd–12% CeO_2–Al_2O_3, which provides a low ignition temperature (240°C). Its high activity is due to the high degree of dispersion of palladium oxide ($D < 250$ Å). The eggshell Pd distribution over the grain cross section is achieved by using $Pd(NO_3)_2$ as the precursor of the active component.

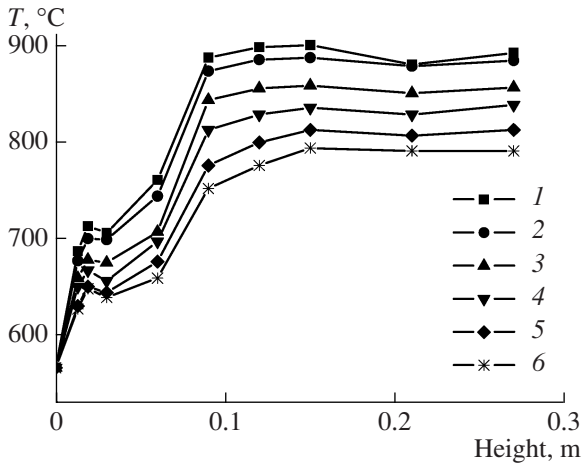

Fig. 10. Temperature profile along the bed height for the combined catalytic package (20 mm IK-12-60-2/20 mm inert material/260 mm IKT-12-40A) at an inlet temperature of 567°C and α = (*1*) 6.68, (*2*) 6.98, (*3*) 7.52, (*4*) 8.11, (*5*) 8.98, and (*6*) 10.00.

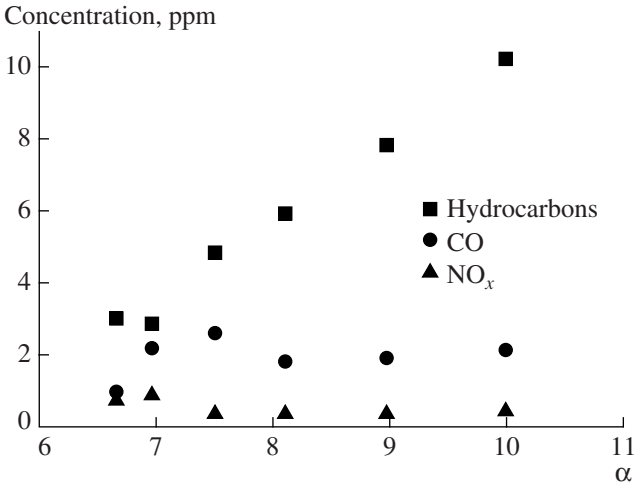

Fig. 11. Unburned hydrocarbons, CO, and NO_x emissions for the combined catalytic package (20 mm IK-12-60-2/20 mm inert material/260 mm IKT-12-40A) as a function of α at an inlet temperature of 567°C.

(2) Thermally stable catalysts based on manganese oxides and hexaaluminates. Their thermal stability is due to the presence of high-temperature phases resulting from the interaction between the active component and the support, as well as solid solutions or manganese hexaaluminate.

The kinetics of methane oxidation on the catalysts was studied, and combustion in the CC was simulated for various catalytic packages and methane combustion conditions. The CC design was optimized based on these calculations. The calculated data are in satisfactory qualitative agreement with the CC testing data.

In the combined catalytic package developed, the highly active Pd catalyst initiates fuel–air mixture ignition. It is placed in the inlet zone of the catalytic package and occupies 7–15% of the total height of the package. The main part of the catalytic package is occupied by an alumina–manganese catalyst. Tests in the optimal CC operating regimes have demonstrated that the process is environmentally quite appropriate: the NO_x concentration in the combustion products is 0–1 ppm, the carbon monoxide concentration is 2–3 ppm, and the unburned hydrocarbon concentration is 3–10 ppm.

ACKNOWLEDGMENTS

This work was supported by Integration Projects within the Program of the Presidium of the Russian Academy of Sciences (grant nos. 7.2 and 7.4), the Russian Foundation for Basic Research (grant nos. 06-08-00981 and 07-08-12272), and government contract no. 02.526.12.6003.

REFERENCES

1. Trimm, D.L., *Appl. Catal.*, 1983, vol. 7, p. 249.
2. Ismagilov, Z.R., Kerzhentsev, M.A., and Susharina, T.L., *Usp. Khim.*, 1990, vol. 59, p. 1676
3. Ismagilov, Z.R. and Kerzhentsev, M.A., *Catal. Today*, 1999, vol. 47, p. 339.
4. Anson, D., Decorso, M., and Parks, W.P., *Int. J. Energy Res.*, 1996, vol. 20, p. 38.
5. Belgian Patent 814752, 1974.
6. Pfefferle, W.C., *J. Energy*, 1978, vol. 2, p. 142.
7. Dalla Betta, R.A. and Rostrup-Nielsen, T., *Catal. Today*, 1999, vol. 47, p. 369.
8. Arai, H., Yamada, T., Equchi, K., and Seiyama, T., *Appl. Catal., A*, 1986, vol. 26, p. 265.
9. Burch, R. and Hayes, M.J., *J. Mol. Catal. A*, 1995, vol. 100, p. 13.
10. Lee, J.H. and Trimm, D.L., *Fuel Process. Technol.*, 1995, vol. 42, p. 339.
11. McCarty, J.G., Gusman, M., Lowe, D.M., Hildenbrand, D.L., and Lau, K.N., *Catal. Today*, 1999, vol. 47, p. 5.
12. Farrauto, R.J., Hobson, M.C., Kennelly, T., and Waterman, E.M., *Appl. Catal., A*, 1992, vol. 81, p. 227.
13. Burch, R., *Pure Appl. Chem.*, 1996, vol. 68, p. 377.
14. McCarty, J.G., *Catal. Today*, 1995, vol. 26, p. 283.
15. Su, S.C., Carstens, J.N., and Bell, A.T., *J. Catal.*, 1998, vol. 176, p. 125.
16. Carstens, J.N., Su, S.C., and Bell, A.T., *J. Catal.*, 1998, vol. 176, p. 136.
17. Lyubovsky, M. and Pfefferle, L., *Appl. Catal., A*, 1998, vol. 173, p. 107.
18. Lyubovsky, M. and Pfefferle, L., *Catal. Today*, 1999, vol. 47, p. 29.
19. Baldwin, T.R. and Burch, R., *Appl. Catal.*, 1990, vol. 66, p. 337.
20. McCarty, J.G., Wong, V.L., and Chang, Y.-F., *Scr. Metall. Mater.*, 1994, vol. 31, p. 1115.

21. Groppi, G., Cristiani, C., Lietti, L., Ramella, C., Valentini, M., and Forzatti, P., *Catal. Today*, 1999, vol. 50, p. 399.
22. Ismagilov, Z.R., Kerzhentsev, M.A., Sazonov, V.A., Tsykoza, L.T., Shikina, N.V., Kuznetsov, V.V., Ushakov, V.A., Mishanin, S.V., Kozhukhar, N.G., Russo, G., and Deutschmann, O., *Korean J. Chem. Eng.*, 2003, vol. 20, p. 461.
23. Ozawa, Y., Tochihara, Y., Nagai, M., and Omi, S., *Chem. Eng. Sci.*, 2003, vol. 58, p. 671.
24. Liotta, L.F. and Deganello, G., *J. Mol. Catal. A: Chem.*, 2003, vols. 204–205, p. 763.
25. Yue, B., Zhou, R., Wang, Y., and Zheng, X., *Appl. Catal., A*, 2005, vol. 295, p. 39.
26. Machida, M., Eguchi, K., and Arai, H., *J. Catal.*, 1987, vol. 103, p. 385.
27. Machida, M., Eguchi, K., and Arai, H., *J. Catal.*, 1989, vol. 120, p. 377.
28. Chouldhary, T.V., Banerjee, S., and Choudhary, V.R., *Appl. Catal., A*, 2002, vol. 234, p. 1.
29. Jang, B.W.- L., Nelson, R.M., Spivey, J.J., Ocal, M., Oukaci, R., and Marcelin, G., *Catal. Today*, 1999, vol. 47, p. 103.
30. Yashnik, S.A., Ismagilov, Z.R., Kuznetsov, V.V., Ushakov, V.V., Rogov, V.A., and Ovsyannikova, I.A., *Catal. Today*, 2006, vol. 117, p. 525.
31. Tsyrul'nikov, P.G., Sal'nikov, V.S., Drozdov, V.A., Stuken, S.A., Bubnov, A.V., Grigorov, E.I., Kalinkin, A.V., and Zaikovskii, V.I., *Kinet. Katal.*, 1991, vol. 32, p. 439.
32. RF Patent 2 185 238, 2002.
33. Tsikoza, L.T., Ismagilov, Z.R., Ushakov, V.A., Kuznetsov, V.V., and Ovsyannikova, I.A., *Kinet. Katal.*, 2003, vol. 44, no. 6, p. 879 [*Kinet. Catal.* (Engl. Transl.), vol. 44, no. 6, p. 806].
34. Dalla Betta, R.A., Schlatter, J.C., Yee, D.K., Loffler, D.G., and Shoji, T., *Catal. Today*, 1995, vol. 26, p. 29.
35. Garroni, R., Griffin, T., Mantzaras, J., and Reinke, M., *Catal. Today*, 2003, vol. 83, p. 157.
36. US Patent 6015285, 2000.
37. Malinovskaya, O.A., Beskov, V.S., and Slin'ko, M.G., *Modelirovanie kataliticheskikh protsessov na poristykh zernakh* (Modeling of Catalytic Processes on Porous Grains), Novosibirsk: Nauka, 1975.
38. Pavlov, K.F., Romankov, P.G., and Noskov, A.A., *Primery i zadachi po kursu protsessov i apparatov khimicheskoi tekhnologii* (Exercises and Problems in Chemical Engineering Science), Leningrad: Khimiya, 1969.
39. Aerov, M.E., Todes, O.M., and Narinskii, M.A., *Apparaty so statsionarnym zernistym sloem: Gidravlicheskie i teplovye osnovy raboty* (Fixed-Bed Apparatuses: Hydraulic and Thermal Principles of Their Operation), Moscow: Khimiya, 1979.
40. *Spravochnik khimika* (Chemist's Handbook), Moscow: Khimiya, 1962–1966, vols. 1–5.
41. Parmon, V.N., Ismagilov, Z.R., Favorskii, O.N., Belokon, A.A., and Zakharov, V.M., *Vestn. Akad Nauk*, 2007, vol. 77, p. 819.